Detailed structural analysis of digital outcrops: A learning example from the Kermanshah-Qulqula radiolarite basin, Zagros Belt, Iran

Adam J. Cawood [a,*], Amerigo Corradetti [b], Pablo Granado [c], Stefano Tavani [d,e]

[a] Space Science and Engineering Division, Southwest Research Institute, 6220 Culebra Rd., San Antonio, Texas, USA
[b] Dipartimento di Matematica e Geoscienze, Università Degli Studi di Trieste, Via Weiss 2, 34128, Trieste, Italy
[c] Institut de Recerca Geomodels, Departament de Dinàmica de La Terra I de L'Oceà, Universitat de Barcelona, C/ Martí I Fraques s/n, 08028, Barcelona, Spain
[d] DISTAR, Università Degli Studi di Napoli "Federico II,", Via Cupa Nuova Cintia 21, 80126, Naples, Italy
[e] Consiglio Nazionale Delle Ricerche, IGAG, c.o. Dipartimento di Scienze Della Terra, Università di Roma Sapienza, P.le Aldo Moro 5, 00185, Roma, Italy

ARTICLE INFO

Keywords:
Zagros
Digital outcrop
Kinematic restoration
Geoscience education
Structural analysis

ABSTRACT

A digital outcrop example and associated structural analysis of highly deformed sedimentary strata from the Zagros Belt of Iran is presented. By providing this site in open-access, downloadable format, we aim to make this excellent outcrop exposure accessible to a wide range of geoscientists. Digital data extraction techniques are used to constrain structural interpretations and cross section orientation, as well as kinematic restorations of interpreted structures. Structural analysis protocols provided here are well-suited to learning outcomes associated with digital cross section construction, interpretation and restoration. Complex deformation at the study locality and associated uncertainties in horizon and fault mapping yield interpretation and structural restoration results that are likely non-unique. Interpretation uncertainties are discussed in the context of geoscience education, with specific reference to the need for considering and assessing data quality and underlying geological assumptions. Our workflow and results can be used to bridge the gap between field-based training at undergraduate level and the proficiency in 3D digital environments required of professional geoscientists. By using digital outcrops to achieve learning outcomes, knowledge of underlying geological processes and practical skills in digital data handling and treatment can be effectively communicated to future geoscientists within the virtual environment.

1. Introduction

The last decade has seen a rapid increase in the use of digital photogrammetry as a tool for reconstructing the natural world in 3D. Improved reconstruction algorithms (e.g., Brown and Lowe, 2005; Furukawa and Ponce, 2009; Wu, 2011), the use of control data (e.g., James and Robson, 2012) and improvements in acquisition workflows (e.g. Bemis et al., 2014; Corradetti et al., 2021) allow highly accurate photogrammetric reconstructions to be generated and used for quantitative structural analysis (e.g., Cawood et al., 2017). Photogrammetric reconstruction of outcrops is now possible with relatively inexpensive consumer-grade equipment and digital photogrammetry software that requires little user expertise. As a result, structural geologists are now able to routinely build digital outcrops and extract a variety of structural data from them. Structural data that can be extracted from digital outcrops include strike and dip measurements (e.g., Tavani et al., 2016), 3D geometric properties of bedding and fault surfaces (Pearce et al., 2011), fault displacement data (e.g., Martinelli et al., 2020), and highly detailed fracture maps (e.g., Bisdom et al., 2014). The ability to collect digital measurements from outcrop has led to a revolution in the way that field-based structural characterization is carried out, and allows for more efficient, safer data collection and the ability for improved sampling of structural data in the field (Biber et al., 2018).

In addition to the potential for digital photogrammetry to provide quantitative structural data, digital outcrops can be important tools for geoscience education (e.g. Pringle, 2014; De Paor, 2016; Houghton et al., 2016; Carbonell Carrera and Bermejo Asensio, 2017; de Paz-Álvarez et al., 2021). Digital outcrops have the potential to improve geological 3D thinking and can provide a mechanism to improve equality, inclusion and diversity in geoscience education and training (Bond and Cawood, 2021). Photogrammetric reconstruction is often cited as being important for providing geological data in difficult-to-reach locations (Vasuki et al., 2014; Franceschi et al., 2015); in the context of geoscience education, digital outcrops can allow

* Corresponding author.
E-mail address: acawood@swri.org (A.J. Cawood).

Accepted 26 November 2021

students to virtually visit geological outcrops that would otherwise be inaccessible to them (McCaffrey et al., 2010; Whitmeyer et al., 2020). This is important not only because of the safety concerns and financial implications associated with field-based training, but because digital access can improve learning outcomes (e.g., Bond and Cawood, 2021). The issues around physical access to field locations have been magnified by the COVID-19 pandemic, which has limited or prohibited field-based training to all geoscience students, and not only those disadvantaged by traditional barriers to access (Arthurs, 2021).

Irrespective of pandemic-related travel restrictions or barriers to field-based training, there are many outcrops around the world which are simply not accessible to most geoscience students. In this study we present a world-class outcrop from the Lurestan region of Iran. By sharing this roadside outcrop example and making the 3D data freely accessible, we aim to provide a unique open-source dataset that can be used for teaching and learning. Our descriptions and analysis of structural features are used to (i) highlight the potential of our methodology and (ii) provide insights into structural development that can be used as a companion training dataset with the open-source digital outcrop.

2. Geological background

The study site is located in the Lurestan Arc of the SE-verging Zagros belt (Fig. 1). Formation of the Zagros belt initiated during the Late Cretaceous due to NE-directed subduction of the Neo-Tethys ocean and associated continental collision between the Arabian and Eurasian plates (e.g., Berberian and King, 1981; Vergés et al., 2011; Allen, 2021). In the Lurestan Arc, the Zagros belt deformed the Triassic-Early Jurassic Arabian rifted margin (Tavani et al., 2021), which constituted the SW margin of the Neo-Tethys; the tectonic nappes of the Zagros belt essentially trace the architecture of the rifted margin (Wrobel-Daveau et al., 2010). The High Zagros Fault is one of the major thrusts of the collisional orogen, along which the sedimentary cover of the distal portion of the Arabian rifted margin overthrust the proximal domain. In detail, the tectonic pile of the Zagros belt consists of a series of nappes that deform, transport, and stack the different domains of the former Neo-Tethyan rifted margin. These nappes include, from top to bottom (e.g., Tavani et al., 2021): (i) a thin ophiolite nappe; (ii) the Bisotun-Avalon nappe, composed of Mesozoic carbonates deposited onto the Bisotun-Avalon continental ribbon; (iii) the Kermanshah-Qulqula nappe (where the study outcrop is located), composed of Lower Jurassic to Upper Cretaceous limestones, radiolarites, marls, and shales deposited in the Kermanshah-Qulqula deep-water basin, developed between the Arabian margin and the Bisotun-Avalon continental ribbon (Gharib and De Wever, 2010); (iv) continental crust of the Arabian margin which corresponds to the proximal and necking domains of the rifted margin.

The Zagros belt in the Lurestan Arc formed during two shortening stages, which led to the development of two foredeep basins of Maastrichtian-Eocene and Miocene-present day age (Fig. 1; Homke et al., 2009; Saura et al., 2015). The older foredeep is preserved in the footwall of the High Zagros Fault, which is capped by the Paleocene to Miocene continental deposits of the Paleogene Red Bed Series (Koshnaw et al., 2017). This relationship suggests that displacement along the High Zagros Fault occurred during the Late Cretaceous to Paleocene interval (Karim et al., 2011; Vergés et al., 2011; Saura et al., 2015).

3. Study locality

The studied exposure is located in the hanging wall of the High Zagros Fault, along the Javanroud-Salas road, 2 km to the west of the city of Javanroud (Fig. 2). It consists of a N–S oriented 110 m wide outcrop that exposes ribbon cherts that alternate with marls, shales, and thinly bedded silicified limestones of latest Sinemurian-earliest Pliensbachian age, of the Kermanshah-Qulqula basin syn-rift sequence (Tavani et al., 2018). Extensional faults are present across the outcrop, and contractional structures interpreted to post-date extensional faulting include inverted normal faults, buttressing structures, kink-folds, and reverse faults.

An interpreted field photograph at the northern part of the study locality (Fig. 3A) shows a low-angle S-dipping basal extensional fault, with cutoff angles from 20° to 60°, that accommodates >10 m of displacement. N-dipping strata in the hanging wall to this fault are

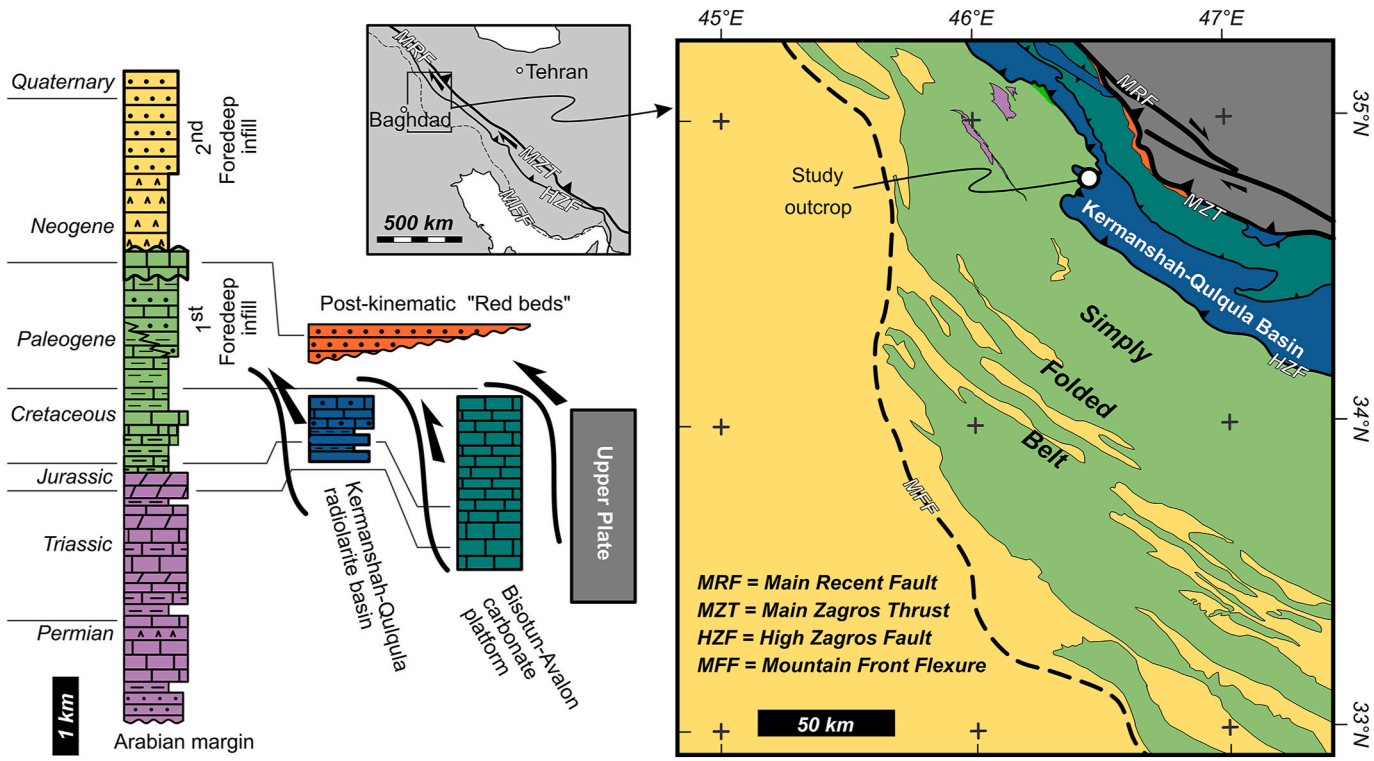

Fig. 1. Geological map and stratigraphic successions of the Lurestan region of the Zagros Belt. Modified after Tavani et al. (2021).

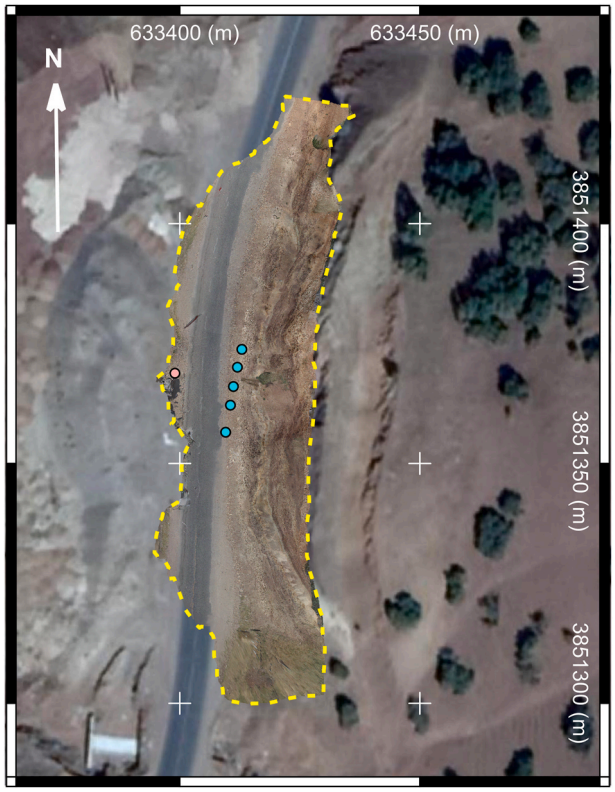

Fig. 2. Co-referenced digital outcrop and satellite imagery. Light blue points denote control point locations. Pink dot shows the location of local reference frame origin. See main text for details. Digital outcrop extents marked by the stippled yellow line. (For interpretation of the references to colour in this figure legend, the reader is referred to the Web version of this article.)

displaced by synthetic S-dipping extension faults (with displacement up to 2 m), and a few small-scale N-dipping antithetic faults. A kink-fold with E-W striking anticlinal and synclinal axial surfaces overlies one of these N-dipping extensional faults.

A squeezed horst structure indicative of buttressing during contraction in the central part of the outcrop (Fig. 3B) is bounded by two N-dipping faults to the north (cut and displaced by a N-verging thrust) and one S-dipping fault to the south. The block to the north displays a much thicker sequence with respect to the southern block, providing evidence for syn-sedimentary displacement along extensional faults at either side of the horst structure. Shaly strata in the horst are tightly folded to form an anticline-syncline-anticline triplet containing steeply dipping strata and E-W striking axial surfaces. Small-scale extensional faults within the horst structure exhibit rotated and folded geometries and as a result display a reverse sense of shear in their present-day configurations.

The southern portion of the outcrop exposes a slightly inverted extensional fault with a ramp-flat geometry (Fig. 3C), with the flat segment of the fault interpreted to have accommodated reverse offset that post-dates extensional displacement. Layers in the footwall of the main fault are highly folded, particularly at the southern edge of the photo, and shales immediately above the main flat are folded too. S-dipping faults with cutoff angles of 50°–60° are characterised by displacements up to 2 m. Their syn-sedimentary nature is evidenced by a remarkable change of thickness, with an overall southward thinning of layers within fault blocks (Fig. 3c).

4. Methods and data

4.1. Field acquisition, data processing and georeferencing

Digital images of the site were acquired using a Nikon D5300, a Canon EOS 450D, and a Canon EOS 1100D. Average ground resolution for acquired imagery was approximately 5.5mm/pixel. Following the procedures described in Tavani et al. (2016), we positioned five targets at a constant elevation using a laser level mounted on a tripod. The position of these targets in a local reference frame was measured in polar coordinates using a compact laser distance meter and a graduated dial whose orientation was registered with a Silva compass. The dial constitutes the origin of this local reference frame and the sixth ground control point (Fig. 2). In addition to digital imagery and ground control data, structural data (i.e., fault and bedding orientations) were also collected manually using compass clinometers. Initial structural interpretations, field sketches and observations were also made as part of the data acquisition campaign.

Photogrammetric processing of outcrop imagery was performed using *Agisoft Metashape 1.7.1*. Initial processing yielded a 3D point-cloud containing approximately 30 million points over a surveyed area of

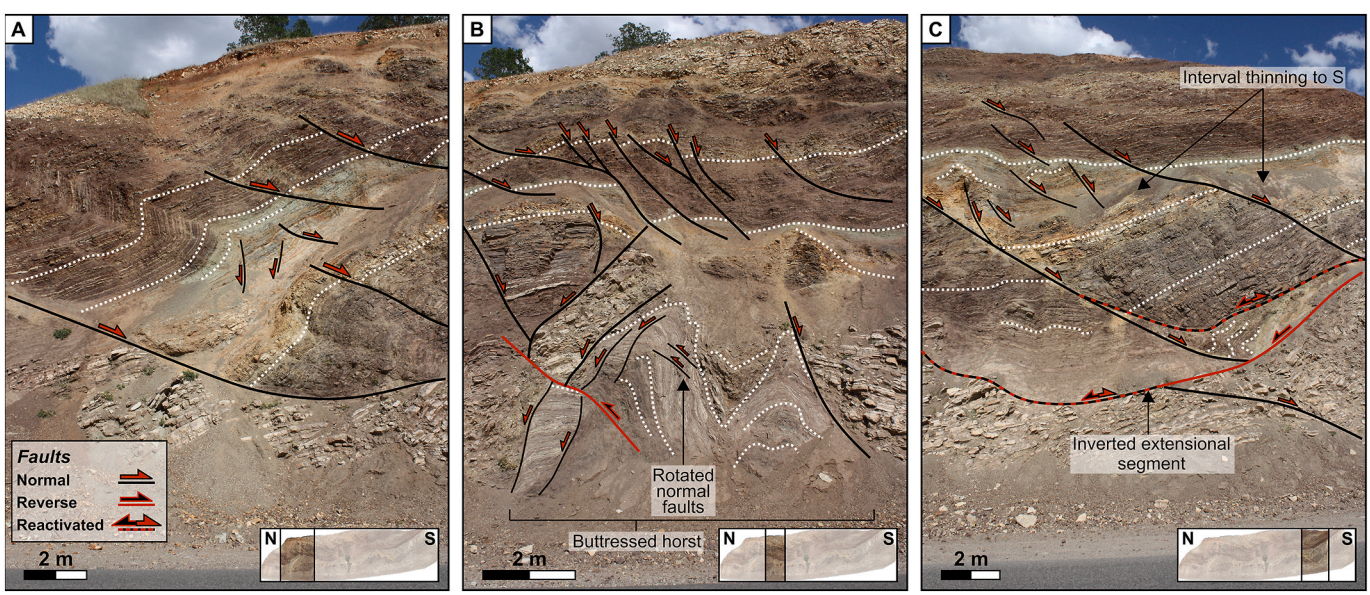

Fig. 3. Interpreted field photographs showing some of the main structural features at the study site. Dotted white horizon markers illustrate structural geometries but are not necessarily used as restoration horizons … See text for detailed structural interpretations.

3095 m^2 (approximate point-cloud density = 1 point/cm^2). The point-cloud was registered through the aforementioned registration scheme using the six ground control points. To improve the registration of the model, we generated in Metashape an orthophoto that was later uploaded in QGIS to optimize the overlap of features by rotating the orthophoto about a vertical axis. The same amount of rotation was then imposed on the model. Later, a textured mesh of the model was exported from Metashape as a Wavefront OBJ (.obj) file prior to data extraction.

4.2. Data extraction, image projection, cross section construction and restoration

The textured outcrop mesh was loaded in Openplot (e.g., Tavani et al., 2016) where portions of exposed bedding and fault traces were used to derive the 3D orientation of these surfaces. The extraction procedure consists in the digitization of polylines from which the software calculates best-fit planes in real-time, allowing the user to evaluate in 3D whether to retain or reject each calculated plane. In essence, this visual evaluation allows the user to discard those planes derived from highly collinear points along digitized polylines. High collinearity of points typically results in best-fit planes that follow outcrop topography rather than the penetrating geometry of the geological features (e.g. Fernández et al., 2009; Jones et al., 2016; Seers and Hodgetts, 2016). A total of 136 planes were extracted from the model (Fig. 4). Bedding data digitized and extracted from the digital outcrop model record a similar best fit plane orientation to that derived from field data (Fig. 4). Note, digitized data display higher orientation dispersion than equivalent field data. We attribute this increase in dispersion to collinearity of points along segments of digitized polylines, and the resultant orientation bias introduced by this collinearity.

Poles to bedding and fault orientation data collected in the field and from the model are plotted in the stereonet in Fig. 4. Through a tensor analysis of the distribution of those poles, in Openplot we calculated the smallest eigenvalue, which corresponds to the direction of minimum concentration of poles. Albeit slightly improperly, we use the term β-axis for this direction, as it averages the direction of the fold axes (i.e., the β-axis) and of intersection with faults structures, being the poles to bedding aligned along their distribution (the so called π;-plane; Ramsay and Huber, 1987).

Both stereonets (from field and digital data) show a distribution of poles along a N–S direction, with a plunging of the β-axis toward the East (94° trend and 36° plunge for the field data and 97° trend and 37.5° plunge for the digitized data). In essence, this statistical direction is the direction toward which we can look at the outcrop with distortions in the geometry of the structures reduced as much as possible (Fig. 5). For this reason, we generated an orthophoto of the model using the calculated β-axis as view direction in Metashape, producing a photorealistic cross section of the outcrop with minimum geometrical distortions (Fig. 6A). Unfortunately we were not able to identify any direct kinematic indicators (e.g., slickenlines on fault planes) at the study site to constrain appropriate cross section orientation. Our cross section strike of 184° (orthogonal to 94° trend of field data), however, is in general agreement with previously published transport directions of NE-SW for both extension and subsequent contraction in the Lurestan region of the Zagros (Vergés et al., 2011; Tavani et al., 2021).

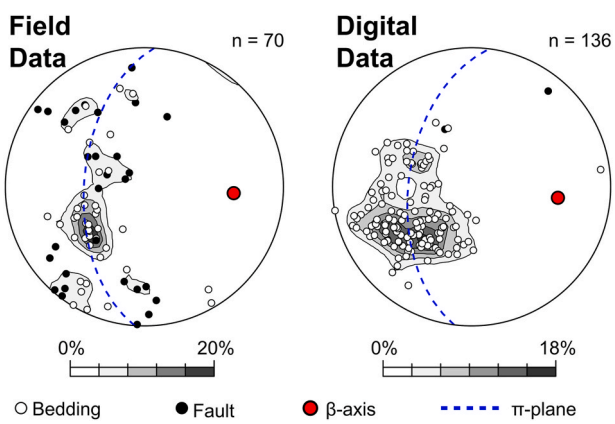

Fig. 4. Structural data collected in the field and digitized on the digital outcrop, with best fit π-plane and β axis extracted with Openplot software (e.g., Tavani et al., 2016) to derive the view direction for orthorectification.

Initial interpretations of structural geometries at the study site were produced from field observations and sketches during fieldwork in 2016, as shown in section 3. Subsequent structural interpretations were derived by interpretation of structural geometries on the photorealistic, orthorectified cross section (Fig. 5A). While each dataset was important for generating structural interpretations, the photorealistic, orthorectified cross section was used to generate final interpretations and to quality check results from 3D digital interpretation. The orthorectified cross section was chosen as the most representative image of the site as it provides a medium for structural interpretation with reduced potential for viewpoint bias and associated geometric inaccuracies (e.g., Tavani et al., 2016). After structural interpretation of the orthorectified cross section, digitized bed boundaries and faults were imported into MOVE 2019.1 for kinematic restoration. Faults and folds were sequentially restored along the cross section using available algorithms in MOVE 2019.1, with both bed length and bed thickness variations allowed through the sequential restoration.

5. Structural interpretation and restoration

The study outcrop is characterised by widespread extensional faults and a few contractional structures. Extensional faults include: (i) almost linear fault strands with limited (<2 m) displacement, which are generally confined within the more competent beds, and (ii) larger extensional faults with >2 m displacement characterised by ramp-flat

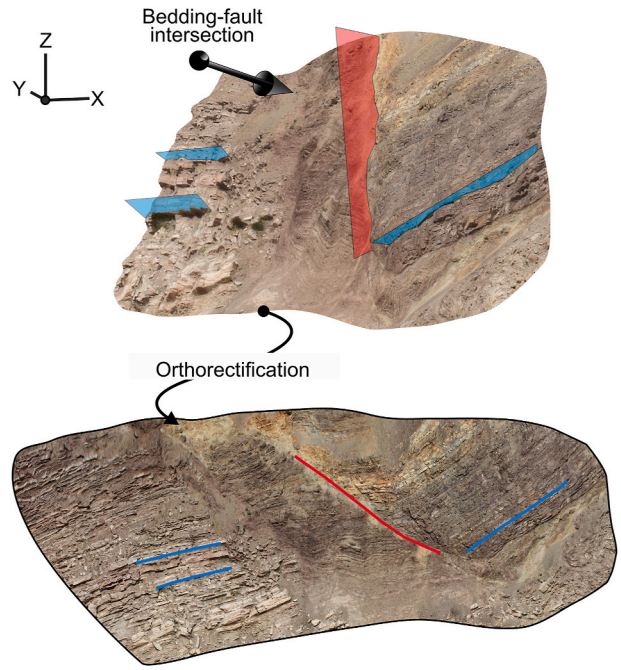

Fig. 5. Procedure for the orthorectification of the digital outcrop along the β-axis. The procedure involves recognition of geological features in the model and computation of the viewing direction of interest, which in the image corresponds to the intersection between bedding (blue) and faults (red), to produce an orthorectified image. (For interpretation of the references to colour in this figure legend, the reader is referred to the Web version of this article.)

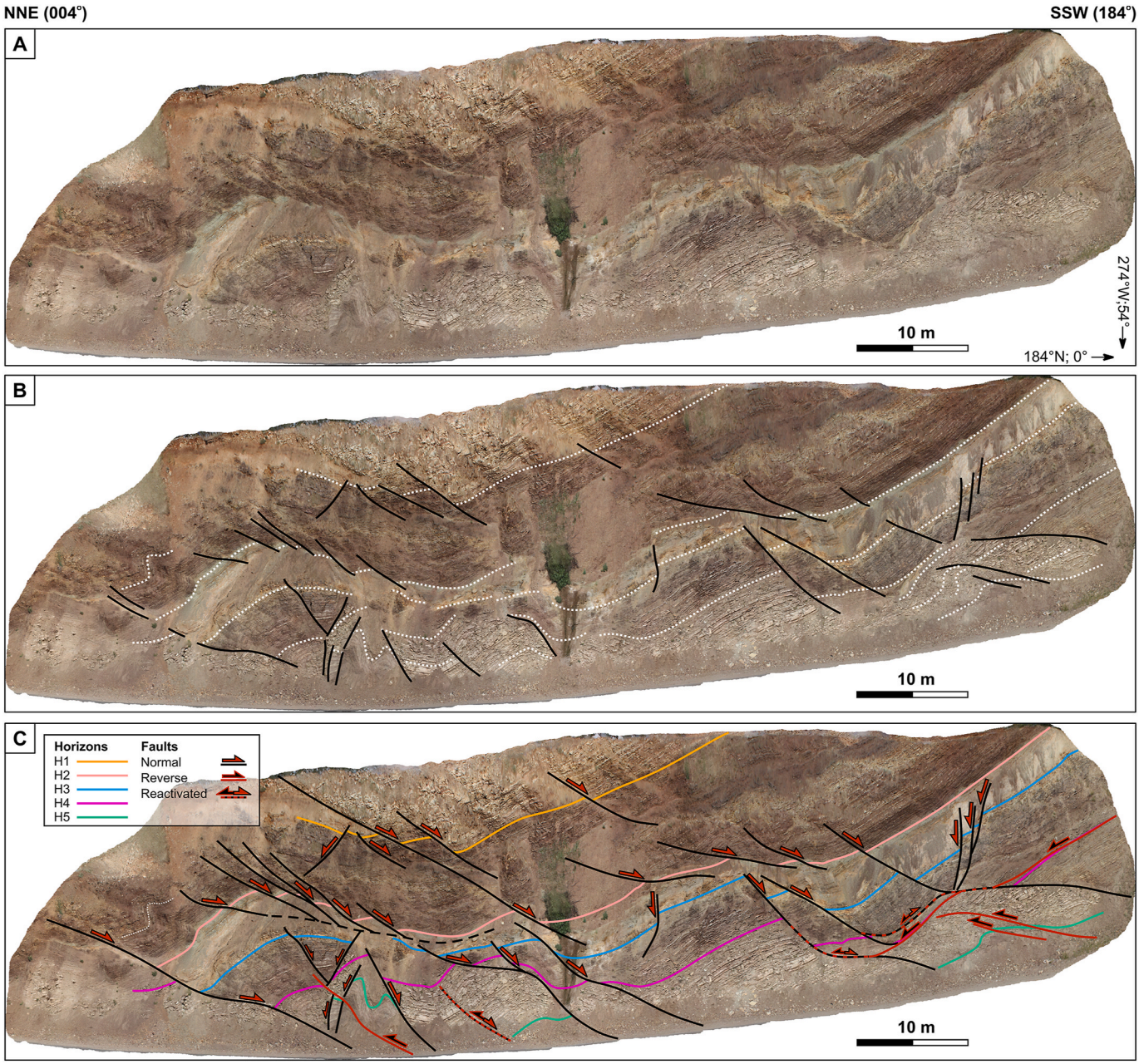

Fig. 6. (A) Orthorectified image of the study locality. Orientation values at bottom right denote trend and plunge of image axes. (B) Intermediate interpretation with only directly observed fault segments and horizons shown. No interpretations of fault offset or correlations between exposed horizons are made. (C) Structural interpretation of the orthorectified image, with horizons and faults interpolated across zones of poor exposure. Interpretations in (C) used for the structural restoration (Fig. 7).

geometries and with associated hanging wall synclines and rollover anticlines. Limited contractional deformation postdating extensional faulting is evidenced by buttressing structures, kink-folds, and scarce reverse faults with displacement in the order of a few cm. Bedding surfaces measured in the field strike approximately E-W (Fig. 4) and, coherently, faults are E-W striking too.

Field observations and interpretation of unreferenced imagery (Fig. 3) were used to guide structural interpretation of the orthorectified outcrop image (Fig. 6A). In detail, many layers and faults can be traced with confidence (Fig. 6B) where correlation between layers across different blocks is evident. In other cases, the correlation is driven by the coarse preservation of horizon lengths and stratal thicknesses. As such, the interpretations shown in Fig. 6C represent a hybrid of directly observed geometries and interpolations where poor exposure hampered direct interpretation. Five key layers have been traced and correlated across the three main fault systems affecting the study outcrop (Fig. 6B). These layers identify different sedimentary packages which area generally represented by shale intervals, with the exceptions of the H3–H4 and H4–H5 packages, which are interpreted as radiolarites and silicified limestones, respectively. The northern fault system includes a main gently SSW-dipping extensional fault, which has in its hanging wall a rollover anticline bounded to the south by the previously mentioned buttressed horst structure. The central fault system is composed of three main segments: the northern one affects the previously illustrated rollover anticline, and at its northern termination the fault splays off in a set of S-dipping extensional faults displacing the horizon H2, whereas to the south this fault segment is folded by a footwall anticline; the southern segments are almost straight and affect

the entire multilayer, with an overstep area located between the horizons H2 and H3.

The third and southernmost fault system is made by three major S-dipping faults affecting horizons H2 to H5, the southernmost fault of this system has an associated antithetic fault system and the northern tips of all of the three faults is overlain by a few subsidiary synthetic faults affecting horizons H1 and H2. The traced horizons show remarkable thickness variations. Part of these variations are attributable to local folds associated with contraction and possibly to uncertainties in the correlation of layers. However, the overall northward wedging of the package delimited by horizons H1 and H2, the thickness variation of the H2-to-H4 package across the southern fault system, and the thickness variation of the H3-to-H5 package across the central fault system and across the squeezed horst, point to a syn-sedimentary nature for the three main fault system and of the extensional faults in general.

Kinematic restoration of structural interpretations was carried out using a two-stage restoration approach. Contractional deformation was restored in the first stage by (i) removing reverse displacement along interpreted thrust faults, and (ii) unfolding the deformed sequence to an interpreted pre-contraction structural configuration (Fig. 7B). The first restoration step is interpreted to be of limited precision because of (i) uncertainties in the amount of contractional reactivation along extensional faults, and (ii) difficulties in distinguishing between contractional and extensional fault-related folding. In spite of these uncertainties, approximate restoration from the present-day to pre-contractional time step provides a general overview and potential scenario for structural configurations at the study site between Triassic-Early Jurassic and Late Cretaceous that is consistent with regional structural interpretations (e.g., Vergés et al., 2011; Saura et al., 2015; Tavani et al., 2018). Clockwise rotation of strata as part of the restoration (Fig. 7B), for example, restores interpreted strata to approximately horizontal at the pre-contractional restoration step and removes the tilting of strata due to folding in the hanging-wall of the High Zagros Fault (e.g., Tavani et al., 2021).

Structural restoration allowed us to observe and interpret the main features of the studied outcrop in the Zagros belt. An initial clockwise rotation of the beds and faults using as datum the youngest horizon (orange marker bed H1; Fig. 7) highlights the occurrence of a south-dipping fault system arranged in ramp - flat strands. Most of the bed offsets across faults are extensional; no significant faults (slip >2 m) with a reverse offset have been found. The restoration of marker horizons to horizontal highlights stratigraphic wedging across normal faults (Fig. 7B), which indicates a syn-sedimentary origin for the fault array. A certain amount of structural decoupling is also observed along the layers between horizons H2 and H3; this is evident for both the extensional faults with several small extensional faults soled at this level. Kink-style folds involving layers above marker horizon H2 also provide evidence for the same decoupling within shaly layers between marker beds H2 and H3 being active during subsequent contractional deformation. Buttressing (and internal deformation) are evident in the multilayered sequences between marker beds H4 and H5 at either ends of the orthorectified cross section (Fig. 5) as well as within the less competent layers (Fig. 6B).

The second stage of restoration, from a post-extension time step (Fig. 7B) to a pre-deformed configuration (Fig. 7C), shows the effects of removing displacement along extensional faults and unfolding marker horizons to horizontal. Variations in line-length of fully restored marker horizons (Fig. 7C) are attributed to (i) variable exposure of sedimentary layers at outcrop and poor exposure of horizon H1 (see Fig. 5), (ii) a structural decoupling level with low angle extensional detachments between horizons H2 and H3, and (iii) systematic increases in extensional displacement downwards through horizons H3, H4 and H5, resulting in progressively shorter line lengths as the H3 to H5 markers are restored. As with the previous restoration step, restored geometries and line lengths shown in the fully restored cross section (Fig. 7C) are approximate.

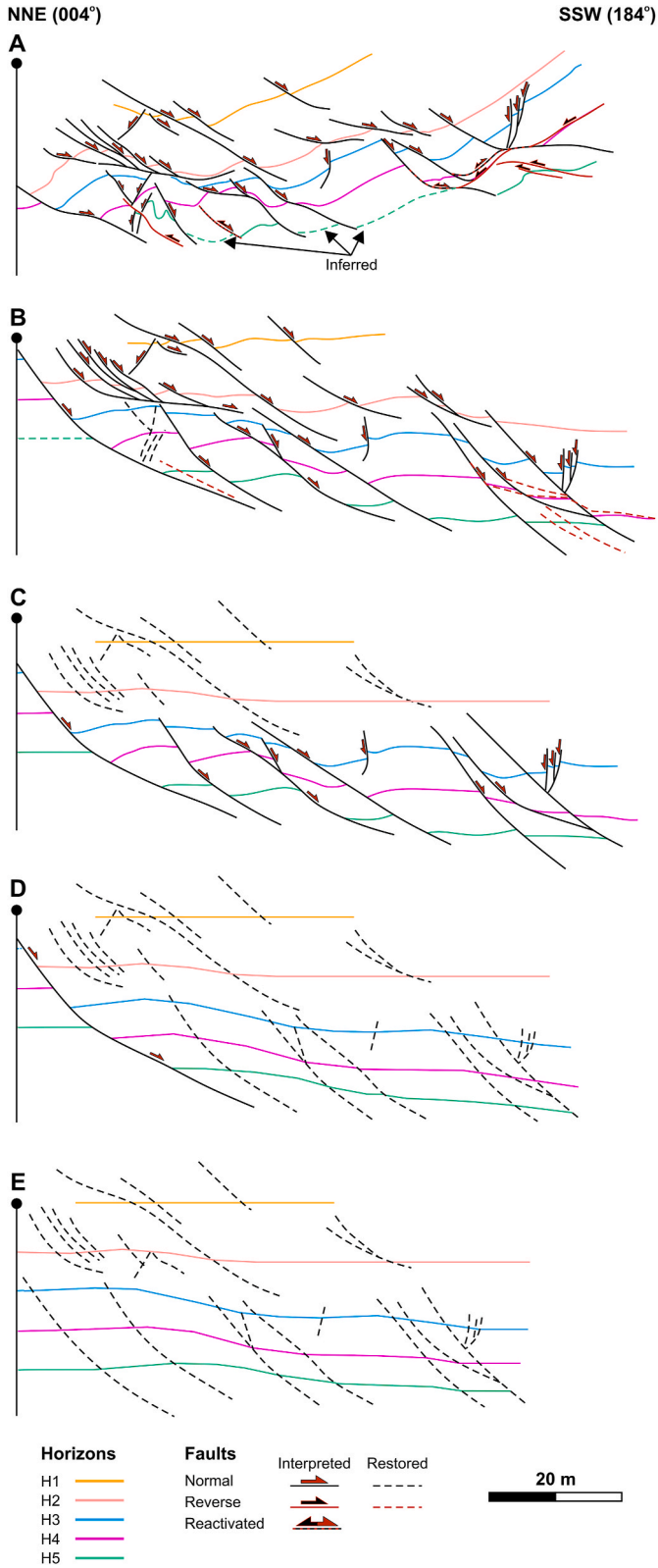

Fig. 7. Kinematic restoration of structural interpretations. (A) Structural interpretation of study locality in 2D, present-day. (B) Partially restored structural interpretation with contractional structures restored and regional tilt removed. (C–E) Progressive restoration of extension in marker horizons.

Interpreted and restored fault geometries (Fig. 7) are interpreted to capture, to some degree, the mechanical properties of the deformed multilayer at the study site. Fault segments exhibit relatively steep dips in the H3–H4 interval, which consists of relatively competent radiolarites, whereas in the relatively incompetent layers above and below, fault segments are generally shallowly dipping or even sub-parallel to bedding. Observed deformation patterns at the site represent a syn-sedimentary extensional fault array whose hanging walls and footwalls have both undergone compressional deformation, as expressed by the buttressing of layers against rigid fault blocks, enhanced by lithological contrasts. The northward tilting of the whole structural suite indicates broad scale folding, most likely associated with the contractional reactivation of an underlying fault system kinematically linked to the former master extensional fault.

6. Discussion

The digital outcrop, structural interpretations and kinematic restoration results shown here are the result of a single day of fieldwork by two of the authors in 2016. Due to logistical constraints, we have been unable to revisit the site since the initial field campaign and our results, therefore, were predominantly derived through digital data extraction and analysis. This scenario is not uncommon in field-based geological research, or industry exploration campaigns, where a field locality is only accessed for a short period of time, and not revisited because of practical or financial limitations. The workflow and results outlined in this study provide a general protocol to (i) digitally capture and preserve outcrop localities that may be difficult to access or revisit in the future, (ii) digitally extract accurate and representative geometric properties from outcrop needed for detailed structural analysis, (iii) carry out quantitative structural characterization of a site using digitally extracted measurements, without the need to revisit the site, and (iv) provide accurately scaled and oriented digital outcrops in an open-access, downloadable format (https://bit.ly/3xVwPCP) as a resource for teaching and learning in geoscience education.

Although upscaling of observations from outcrop scale to the scale of the thrust belt should be always done with caution, structures illustrated in this work neatly summarize the evolution of this portion of the Zagros Belt, from Mesozoic rifting to Cretaceous-Tertiary inversion tectonics. The syn-sedimentary extensional faults documented here affect the Sinemurian-Pliensbachian deep-water infill of the Kermanshah-Qulqula radiolarite basin (forming part of the Arabian rifted margin) (e.g. Tavani et al., 2018), evidencing that after syn-rift crustal thinning and drowning of the substratum below the carbon compensation depth, the basin was still actively extending. In agreement, hyper-extension in this area eventually evolved to mantle exhumation (Wrobel-Daveau et al., 2010). Convergence and incorporation of the Arabian rifted margin into the Zagros Belt started during the Late Cretaceous (e.g. Vergés et al., 2011), leading to the positive inversion of inherited faults. Such an inversion tectonics stage is here evidenced by limited reverse reactivation of extensional faults and, above all, by buttressing structures such as those illustrated in our structural interpretations of the study locality (Figs. 3 and 6).

Our workflow and associated data provide a general protocol for digital outcrop-based structural analysis through building and restoring a geological cross section. Cross section construction and restoration is a commonly used approach for understanding the effects of deformation and the temporal evolution of structures (e.g, Ramsay and Huber, 1987). By downloading, interpreting and analyzing the digital outcrop provided here, students can digitally generate and analyze their own geological cross sections and gain practical experience in this commonly used approach to understanding deformation processes. In doing so, they can learn first-hand the techniques for digitally manipulating and analyzing structural data (e.g., geometric projection of structural data, generating and assessing best fit planes to polyline traces), and use these data to decipher the deformation processes that result in present-day structural configurations at outcrop. Understanding the limitations of different data types (e.g., digital vs. field-derived structural measurements, Fig. 4) is another potentially important learning outcome that can be communicated through digital outcrop-based exercises. By comparing field data with digital measurements (e.g., Jones et al., 2016), students can be encouraged to consider how reliable and representative data may be, and to think more broadly about how to mitigate against error during data acquisition (e.g., Cawood et al., 2017) and analysis (e.g., Bisdom et al., 2014).

Implicit in any structural interpretation and cross section restoration are assumptions about mechanisms of deformation, mechanical properties of rock layers, and pre-deformation geometries (e.g., Woodward et al., 1989). The interpretations and restoration steps provided here do not represent unique solutions to the structural evolution of the study site. Rather, we suggest that our data and interpretations can be used, through focused structural interpretation and discussion exercises, as a tool for geoscience education. Additional insights into the syn-sedimentary fault system and related depositional history could be gained by time-stepped sequential restorations of the stratigraphic packages, for instance.

Discussions and teaching exercises related to these factors and the influence they have on deformation processes could be focused on the 3D examples shown in this study. Despite the high resolution of the generated orthomosaic (Fig. 6), identifying and interpolating faults and horizons was not always straightforward; imperfect outcrop exposure and complex structural configurations (not easily restored or modelled) presented uncertainties in the structural interpretation. Uncertainties related to the interpretation of faults or lithological contacts are commonplace in the geosciences (Bond, 2015), from undergraduate field-based mapping exercises (e.g., Petcovic et al., 2009) to the interpretation of seismic data for industrial applications (e.g, Alcalde et al., 2017). By using a digital version of an outcrop example, these uncertainties can be highlighted in the virtual environment, and students can gain hands-on experience of digitally adjusting and refining their interpretations in 3D, as is common when interpreting seismic data, or constructing and restoring cross sections.

Digital outcrops can be used to transfer the knowledge gained from field and classroom-based training at undergraduate level to the 3D digital environments that are commonplace in the applied geosciences. Blended learning exercises based around digital outcrops have been shown to improve 3D thinking in the geosciences (e.g., Bond and Cawood, 2021). By designing and implementing digital outcrop-based teaching approaches (e.g., Houghton et al., 2016; Carbonell Carrera and Bermejo Asensio, 2017), improvements in 3D thinking can be further leveraged to incorporate understanding of fundamental geological principles with training in digital data handling and analysis (McCaffrey et al., 2005). As noted by Dolphin et al. (2019), there should be greater emphasis in geoscience education on how geology works rather than simply what it is. The approach suggested here will allow students to learn both established geological theory and the 3D digital skills required in the applied geosciences. This will equip students with an understanding of fundamental geological processes and the practical, digital skills required of modern-day researchers and applied geoscientists.

7. Conclusions

We present a digital outcrop example of highly deformed sedimentary strata from the Zagros Belt of Iran. This site is not easily accessible to most geoscientists and by providing the digital outcrop in open-access, downloadable format, we aim to make this spectacular outcrop accessible to the wider geoscience community.

Digital data extraction techniques are used to constrain the orientation of a geological cross section, associated structural interpretations, and kinematic restoration of the interpreted structures. The digital outcrop and structural analysis steps provided here are well-suited to

teaching cross section construction and interpretation using digital datasets.

Complex deformation at the study site and associated difficulties in horizon and fault interpretation yield results that are likely non-unique. Interpretation uncertainties are discussed in the context of geoscience education, and the need for assessment and consideration of data quality and underlying geological assumptions.

Our workflow and associated results can be used to bridge the gap between field-based training and the 3D digital skills required of modern-day geoscientists. By utilizing digital outcrops for teaching and training, both underlying geological knowledge and digital data handling skills can be taught within the virtual environment.

Author statement

Conceptualization: Tavani, Cawood, Corradetti, Granado. **Methodology:** Corradetti, Cawood, Tavani, Granado. **Formal Analysis:** Cawood, Corradetti, Granado, Tavani. **Writing – original draft:** Cawood, Tavani, Corradetti, Granado. **Writing – review and editing:** Cawood, Tavani, Corradetti, Granado.

Declaration of competing interest

The authors declare that they have no known competing financial interests or personal relationships that could have appeared to influence the work reported in this paper.

Acknowledgments

Stefano Tavani and Amerigo Corradetti wish to thank the NIOC staff for field support. Amerigo Corradetti thanks Petroleum Experts for academic use of Move 2019 at the University of Trieste. Pablo Granado was funded by the Institut de Recerca Geomodels and the Grup de Geodinàmica i Analisi de Conques (2014SGR467). Tom Blenkinsop and Ken McCaffrey are thanked for thoughtful, positive, and thorough reviews that improved this paper. Clare Bond and Virginia Toy are thanked for editorial handling.

References

Alcalde, J., Bond, C.E., Johnson, G., Butler, R.W.H., Cooper, M.A., Ellis, J.F., 2017. The importance of structural model availability on seismic interpretation. J. Struct. Geol. 97, 161–171. https://doi.org/10.1016/j.jsg.2017.03.003.

Allen, M.B., 2021. Arabia-Eurasia Collision. Encyclopedia of Geology, pp. 436–450. https://doi.org/10.1016/B978-0-12-409548-9.12522-9.

Arthurs, L.A., 2021. Bringing the field to students during COVID-19 and beyond. GSA Today (Geol. Soc. Am.) 31. https://doi.org/10.1130/GSATG478GW.1.

Bemis, S.P., Micklethwaite, S., Turner, D., James, M.R., Akciz, S., Thiele, S.T., Bangash, H.A., 2014. Ground-based and UAV-Based photogrammetry: a multi-scale, high-resolution mapping tool for structural geology and paleoseismology. J. Struct. Geol. 69, 163–178. https://doi.org/10.1016/j.jsg.2014.10.007.

Berberian, M., King, G.C.P., 1981. Towards a paleogeography and tectonic evolution of Iran. Can. J. Earth Sci. 18, 210–265. https://doi.org/10.1139/e81-019.

Biber, K., Khan, S.D., Seers, T.D., Sarmiento, S., Lakshmikantha, M.R., 2018. Quantitative characterization of a naturally fractured reservoir analog using a hybrid lidar-gigapixel imaging approach. Geosphere 14, 710–730. https://doi.org/10.1130/GES01449.1.

Bisdom, K., Gauthier, B.D.M., Bertotti, G., Hardebol, N.J., 2014. Calibrating discrete fracture-network models with a carbonate three-dimensional outcrop fracture network: implications for naturally fractured reservoir modeling. AAPG Bull. 98, 1351–1376. https://doi.org/10.1306/02031413060.

Bond, C.E., 2015. Uncertainty in structural interpretation: lessons to be learnt. J. Struct. Geol. 74, 185–200. https://doi.org/10.1016/j.jsg.2015.03.003.

Bond, C.E., Cawood, A.J., 2021. A role for virtual outcrop models in blended learning–improved 3D thinking and positive perceptions of learning. Geosci. Commun. 4, 233–244. https://doi.org/10.5194/gc-4-233-2021.

Brown, M., Lowe, D.G., 2005. Unsupervised 3D object recognition and reconstruction in unordered datasets. In: Fifth International Conference on 3-D Digital Imaging and Modeling (3DIM'05), pp. 56–63. https://doi.org/10.1109/3DIM.2005.81.

Carbonell Carrera, C., Bermejo Asensio, L.A., 2017. Augmented reality as a digital teaching environment to develop spatial thinking. Cartogr. Geogr. Inf. Sci. 44, 259–270. https://doi.org/10.1080/15230406.2016.1145556.

Cawood, A.J., Bond, C.E., Howell, J.A., Butler, R.W., Totake, Y., 2017. LiDAR, UAV or compass-clinometer? Accuracy, coverage and the effects on structural models. J. Struct. Geol. 98, 67–82. https://doi.org/10.1016/j.jsg.2017.04.004.

Corradetti, A., Seers, T.D., Billi, A., Tavani, S., 2021. Virtual outcrops in a pocket: the smartphone as a fully equipped photogrammetric data acquisition tool. GSA Today (Geol. Soc. Am.) 31. https://doi.org/10.1130/GSATG506A.1.

De Paor, D.G., 2016. Virtual rocks. GSA Today (Geol. Soc. Am.) 26, 4–11. https://doi.org/10.1130/GSATG257A.1.

de Paz-Álvarez, M.I., Blenkinsop, T.G., Buchs, D.M., Gibbons, G.E., Cherns, L., 2021. Virtual fieldtrip to the Esla Nappe (Cantabrian Zone, NW Spain): delivering traditional geological mapping skills remotely using real data. Solid Earth Discuss. https://doi.org/10.5194/se-2021-110 submitted for publication.

Dolphin, G., Dutchak, A., Karchewski, B., Cooper, J., 2019. Virtual field experiences in introductory geology: addressing a capacity problem, but finding a pedagogical one. J. Geosci. Educ. 67 (2), 114–130. https://doi.org/10.1080/10899995.2018.1547034.

Fernández, O., Jones, S., Armstrong, N., Johnson, G., Ravaglia, A., Muñoz, J.A., 2009. Automated tools within workflows for 3D structural construction from surface and subsurface data. GeoInformatica 13, 291–304. https://doi.org/10.1007/s10707-008-0059-y.

Franceschi, M., Martinelli, M., Gislimberti, L., Rizzi, A., Massironi, M., 2015. Integration of 3D modeling, aerial LiDAR and photogrammetry to study a synsedimentary structure in the early jurassic calcari grigi (southern alps, Italy). Euro. J. Rem. Sens. 48, 527–539. https://doi.org/10.5721/EuJRS20154830.

Furukawa, Y., Ponce, J., 2009. Accurate, dense, and robust multiview stereopsis. IEEE Trans. Pattern Anal. Mach. Intell. 32, 1362–1376.

Gharib, F., De Wever, P., 2010. Mesozoic radiolarians from the Kermanshah formation (Iran). Comptes Rendus Palevol 9, 209–219. https://doi.org/10.1016/j.crpv.2010.06.003.

Homke, S., Vergés, J., Serra-Kiel, J., Bernaola, G., Sharp, I., Garcés, M., Montero-Verdú, I., Karpuz, R., Goodarzi, M.H., 2009. Late Cretaceous–Paleocene Formation of the Proto–Zagros Foreland Basin, Lurestan Province, SW Iran, vol. 121. Geological Society of America Bulletin, pp. 963–978. https://doi.org/10.1130/B26035.1.

Houghton, J., Gordon, C., Craven, B., Robinson, A., Lloyd, G.E., Morgan, D.J., 2016. How to Make a Virtual Landscape with Outcrops for Use in Geoscience Teaching. AGUFM. ED51H-0847.

James, M.R., Robson, S., 2012. Straightforward reconstruction of 3D surfaces and topography with a camera: accuracy and geoscience application. J. Geophys. Res. 117, F03017. https://doi.org/10.1029/2011JF002289.

Jones, R.R., Pearce, M.A., Jacquemyn, C., Watson, F.E., 2016. Robust best-fit planes from geospatial data. Geosphere 12, 196–202. https://doi.org/10.1130/GES01247.1.

Karim, K.H., Koyi, H., Baziany, M.M., Hessami, K., 2011. Significance of angular unconformities between Cretaceous and Tertiary strata in the northwestern segment of the Zagros fold–thrust belt, Kurdistan. Geol. Mag. 148, 925–939. https://doi.org/10.1017/S0016756811000471.

Koshnaw, R.I., Horton, B.K., Stockli, D.F., Barber, D.E., Tamar-Agha, M.Y., Kendall, J.J., 2017. Neogene shortening and exhumation of the Zagros fold-thrust belt and foreland basin in the Kurdistan region of northern Iraq. Tectonophysics 694, 332–355. https://doi.org/10.1016/j.tecto.2016.11.016.

Martinelli, M., Bistacchi, A., Mittempergher, S., Bonneau, F., Balsamo, F., Caumon, G., Meda, M., 2020. Damage zone characterization combining scan-line and scan-area analysis on a km-scale Digital Outcrop Model: the Qala Fault (Gozo). J. Struct. Geol. 140, 104–144.

McCaffrey, K.J.W., Jones, R.R., Holdsworth, R.E., Wilson, R.W., Clegg, P., Imber, J., Holliman, N., Trinks, I., 2005. Unlocking the spatial dimension: digital technologies and the future of geoscience fieldwork. J. Geol. Soc. 162 (6), 927–938.

McCaffrey, K.J.W., Hodgetts, D., Howell, J.A., Hunt, D., Imber, J., Jones, R.R., Tomasso, M., Thurmond, J., Viseur, S., 2010. In: Virtual Fieldtrips for Petroleum Geoscientists. Petroleum Geology Conference Series, vol. 7. Geological Society, London, pp. 19–26. https://doi.org/10.1144/0070019.

Pearce, M.A., Jones, R.R., Smith, S.A., McCaffrey, K.J., 2011. Quantification of fold curvature and fracturing using terrestrial laser scanning. AAPG Bull. 95, 771–794.

Petcovic, H.L., Libarkin, J.C., Baker, K.M., 2009. An empirical methodology for investigating geocognition in the field. J. Geosci. Educ. 57, 316–328. https://doi.org/10.5408/1.3544284.

Pringle, J.K., 2014. Educational egaming: the future for geoscience virtual learners? Geol. Today 30, 147–150.

Ramsay, J.G., Huber, M.I., 1987. The Techniques of Modern Structural Geology: Folds and Fractures. Academic Press, London, UK, p. 700.

Saura, E., Garcia-Castellanos, D., Casciello, E., Parravano, V., Urruela, A., Vergés, J., 2015. Modeling the flexural evolution of the Amiran and Mesopotamian foreland basins of NW Zagros (Iran-Iraq). Tectonics 34, 377–395. https://doi.org/10.1002/2014TC003660.

Seers, T.D., Hodgetts, D., 2016. Probabilistic constraints on structural lineament best fit plane precision obtained through numerical analysis. J. Struct. Geol. 82, 37–47. https://doi.org/10.1016/j.jsg.2015.11.004.

Tavani, S., Corradetti, A., Billi, A., 2016. High precision analysis of an embryonic extensional fault-related fold using 3D orthorectified virtual outcrops: the viewpoint importance in structural geology. J. Struct. Geol. 86, 200–210. https://doi.org/10.1016/j.jsg.2016.03.009.

Tavani, S., Parente, M., Vitale, S., Iannace, A., Corradetti, A., Bottini, C., Morsalnejad, D., Mazzoli, S., 2018. Early Jurassic rifting of the Arabian passive continental margin of the Neo-Tethys. Field evidence from the Lurestan region of the Zagros fold-and-thrust belt, Iran. Tectonics 37, 2586–2607. https://doi.org/10.1029/2018TC005192.

Tavani, S., Granado, P., Corradetti, A., Camanni, G., Vignaroli, G., Manatschal, G., Mazzoli, S., Muñoz, J.A., Parente, M., 2021. Rift inheritance controls the switch from thin- to thick-skinned thrusting and basal décollement re-localization at the subduction-to-collision transition. GSA Bulletin. https://doi.org/10.1130/B35800.1.

Vasuki, Y., Holden, E.-J., Kovesi, P., Micklethwaite, S., 2014. Semi-automatic mapping of geological Structures using UAV-based photogrammetric data: an image analysis approach. Comput. Geosci. 69, 22–32. https://doi.org/10.1016/j.cageo.2014.04.012.

Vergés, J., Saura, E., Casciello, E., Fernàndez, M., Villaseñor, A., Jiménez-Munt, I., García-Castellanos, D., 2011. Crustal-scale cross sections across the NW Zagros belt: implications for the Arabian margin reconstruction. Geol. Mag. 148, 739–761. https://doi.org/10.1017/S0016756811000331.

Whitmeyer, S.J., Atchinson, C., Collins, T.D., 2020. Using mobile technologies to enhance accessibility and inclusion in field- based learning enhance accessibility and inclusion. GSA Today (Geol. Soc. Am.) 30. https://doi.org/10.1130/GSATG462A.1.

Wrobel-Daveau, J.-C., Ringenbach, J.-C., Tavakoli, S., Ruiz, G.M.H., Masse, P., Frizon de Lamotte, D., 2010. Evidence for mantle exhumation along the Arabian margin in the Zagros (Kermanshah area, Iran). Arab. J. Geosci. 3, 499–513. https://doi.org/10.1007/s12517-010-0209-z.

Woodward, N.B., Boyer, S.E., Suppe, J., 1989. Balanced Geological Cross Sections. American Geophysical Union, Short Courses in Geology, vol. 6, p. 132.

Wu, C., 2011. VisualSFM: AVisual structure from motion system. www.cs.washington.edu/homes/ccwu/vsfm/.